Investigation of concrete crack kinematics through probability density field of the location of acoustic emission events

Zhang, Fengqiao; Yang, Yuguang; Hendriks, Max A.N.

DOI
10.1016/j.conbuildmat.2023.132595

Publication date
2023

Document Version
Final published version

Published in
Construction and Building Materials

Citation (APA)
Zhang, F., Yang, Y., & Hendriks, M. A. N. (2023). Investigation of concrete crack kinematics through probability density field of the location of acoustic emission events. *Construction and Building Materials*, *400*, Article 132595. https://doi.org/10.1016/j.conbuildmat.2023.132595

Construction and Building Materials 400 (2023) 132595

Contents lists available at ScienceDirect

Construction and Building Materials

journal homepage: www.elsevier.com/locate/conbuildmat

Investigation of concrete crack kinematics through probability density field of the location of acoustic emission events

Fengqiao Zhang [a,*], Yuguang Yang [a], Max A.N. Hendriks [a,b]

[a] Department of Engineering Structures, Delft University of Technology, 2628CN Delft, The Netherlands
[b] Department of Structural Engineering, Norwegian University of Science and Technology, 7491 Trondheim, Norway

ARTICLE INFO

Keywords:
Probability density of acoustic emission events
Source localization
Concrete structures
Crack kinematics
Digital image correlation

ABSTRACT

Monitoring or identifying structural cracks is crucial for assessing the health of existing concrete structures. Key information about structural cracking encompasses the location of the crack and its kinematics, which include movements perpendicular and parallel to the crack face. Acoustic emission (AE) is a sensitive technique for detecting the location of internal concrete cracking. However, the state-of-the-art AE monitoring methods offer limited information on crack kinematics, restricting the use of AE in crack assessment. To bridge this gap, this paper uses a recently proposed AE data analysis method that quantifies the spatial distribution of AE events along a crack probabilistically. This method uses a parameter referred to as the probability density of AE events (pdAE). By combining pdAE and crack kinematics measured by digital image correlation in a series of real-scale concrete beam tests, this paper investigates the relationship between AE events and crack kinematics. The analysed cracks are generated by a combination of bending moment and shear forces, as commonly observed in real structural concrete members. We find that the amount of AE events is not only related to crack width (the crack movement perpendicular to the crack face), as most literature suggests, but also to the complete crack kinematics throughout the loading history of the member. We then provide a physical explanation for the observed relationships between concrete crack kinematics and the quantity of AE events.

1. Introduction

Many existing concrete structures are nearing the end of their service life [1,2]. Due to increasing load and deterioration of material, the structural capacity may not meet the requirement. Decisions on the interventions to these bridges are needed—whether to demolish, refurbish, or take no action. From sustainable construction perspective, maintenance is preferred. A proper intervention plan requires information on the structural health condition.

Cracking is a typical damage in reinforced concrete structures [3,4]. It may reduce the structural capacity depending on its location and magnitude. According to theoretical models of structural failure, especially those concerning the critical shear failure mode [3,5,6], important indicators of structural capacity are the crack locations and the complete crack kinematics including crack opening and sliding. Crack width is the crack opening in normal direction to the crack faces, and shear displacement refers to the tangential displacement or sliding between the two crack faces.

Various techniques are available to measure concrete cracking, including linear variable differential transformers (LVDT), unmanned aerial vehicles (UAV), digital image correlation (DIC) [7]. Among these, acoustic emission (AE) stands out due to its sensitivity to cracking, its ability to detect internal damages, its real-time crack detection capabilities, and the ease of sensor installation on the structural surface [8].

The basic principle of AE is that concrete cracking releases energy and generates elastic waves from a localized source which is often idealized as a point source [9]. The waves propagate from the source to the AE sensors installed on the surface. By processing the received AE signals, one can estimate the locations of cracks even inside the structural member (which is called source localization [10]), distinguish the source types (which is called source classification [11]) and evaluate the structural integrity [12].

AE has been widely applied in monitoring the cracking conditions of concrete structures, including new [13,14] and existing [15–17] concrete structures. A common observation is that more AE hits/energy are obtained at more severe concrete cracking.

Many experimental studies have attempted to establish a relationship between the amount of AE hits/energy and crack width. Some

* Corresponding author.
E-mail address: F.Zhang-5@tudelft.nl (F. Zhang).

https://doi.org/10.1016/j.conbuildmat.2023.132595
Received 11 May 2023; Received in revised form 20 July 2023; Accepted 21 July 2023
Available online 30 July 2023

researchers propose relating AE energy to the fracture energy of concrete [18,19]. Such relationships are strongly related to the experiments and cannot be extrapolated to other experimental conditions [20,21]. Carpinteri et al. suggested that the AE energy originates from the kinetic energy related to the unstable local snapback during the cracking process of concrete [22,23], which has been implied by some experiments [24,25]. But no direct link has been found between AE energy and crack width.

The studies in the literature focus mostly on relating AE to crack width. But in real-life structural concrete members, concrete cracking can result from more complex actions, including but not limited to bending moments and shear forces. As a result, the relationship between AE events and cracking is not complete without considering both the crack width and the shear displacement between the two crack faces.

Few studies in the literature employ AE to examine the complete kinematics of cracks including crack width and shear displacement. Moment Tensor Analysis (MTA) is a method used to characterize the source of AE, including tensile cracking (Mode I), shear cracking (Mode II) and the mixed mode [26,27]. However, the term 'shear cracking' in MTA refers to the formation of micro-cracks caused by shear stress. The 'shear displacement' that is needed in structural assessments pertains to a next stage where these micro-cracks have evolved into a macro-crack, and frictions occur between the two crack faces due to the shear force. It is this shear displacement that contributes to the shear capacity via aggregate interlock. Close to failure, a large increase of shear displacements is often observed [5] and for a structural assessment it is particularly important to be able to monitor these shear displacements.

Therefor this paper studies the AE events originating from complete crack kinematics using a series of failure tests of large-scale reinforced concrete beams. The analysed cracks include both flexural cracks driven by the tensile stresses at the crack tips and flexural shear cracks driven by a combination of tensile and shear stresses at the crack tips [28]. The crack kinematics were tracked by DIC measurements, and the associated AE signals were recorded. We use a recently proposed AE data analysis method [29] that computes a parameter called probability density of the location of AE events (pdAE). The parameter considers the source localization errors and probabilistically estimates the amount of AE events at a location. Then we compare the pdAE with the crack kinematics obtained from DIC at multiple locations along the cracks. The beams were loaded in cycles during the tests. Therefore, we study different mechanisms in the load cycles: during the loading process, the main mechanisms are crack opening and/or sliding; while during the unloading process, the main mechanisms are crack closure and/or sliding.

This study is unique in several ways: from a data analysis perspective, the pdAE allows for a more realistic quantification of AE spatial distribution, while its association with DIC enables us to relate AE events to local crack mechanisms; from an application perspective, the studied cracks originate from large-scale tests under complex stress states, displaying crack mechanisms comparable to those found in actual concrete structural members.

The results indicate that, unlike idealized small-scale fracture tests focusing on a single fracture mode, both tensile cracking and friction are the dominant AE sources in large-scale structures, particularly within the vast volume of concrete between the reinforcement layers. The amount of AE events should be related to the complete crack kinematics including both crack width and shear displacement, particularly considering their sequence in the crack opening history. The obtained pdAE-crack kinematics relationship allows for a more rational assessment of concrete cracking using AE.

2. Methods

In this section, we introduce the methods employed to estimate the local crack kinematics from DIC measurements (Section 2.1) and the recently proposed AE data analysis method to estimate the local amount of AE events (Section 2.2).

2.1. Estimation of the crack kinematics using DIC

Crack kinematics at a location along a crack refer to crack opening and sliding, or more specifically, the normal and tangential displacements between the two crack faces. The normal displacement is perpendicular to the local crack profile and the tangential displacement is parallel to it. Fig. 1c illustrates the normal and tangential displacements at a location along a crack. Throughout the remainder of this paper, the normal displacement is referred to as the crack width (noted as w), and the tangential displacement is referred to as the shear displacement (noted as Δ).

Crack kinematics can be calculated based on DIC measurement results [30]. The direct output of DIC is the displacement field, which is then converted into the principal strain field (as exemplified in Fig. 7a, which is discussed in Section 3). The obtained strain field reflects the crack pattern. We then approximate the crack pattern to a series of continuous nominal crack segments (Fig. 1a). Each segment has its own angle, representing the angle of the local crack profile (Fig. 1b). Once the differential displacements on both sides of a crack and the angle at a location are known, we can determine the crack kinematics including crack width and shear displacement at that location (Fig. 1c) as

$$\begin{pmatrix} w \\ \Delta \end{pmatrix} = \begin{pmatrix} \sin\alpha & -\cos\alpha \\ \cos\alpha & \sin\alpha \end{pmatrix} \begin{pmatrix} \mathrm{d}x \\ \mathrm{d}z \end{pmatrix} \tag{1}$$

where $\mathrm{d}x$, $\mathrm{d}z$ are the differential displacement of the two crack faces at a local position in $\times$ and z direction respectively, α is the crack angle with respect to the $\times$ direction at the local position, w is the calculated crack width and Δ is the shear displacement.

2.2. Quantification of AE events using probability density function in space domain

To assess the amount of AE events at a location, we first need to localize the AE events using AE source localization techniques [10]. However, due to the localization errors [31], the estimated location may not be the actual one, which impacts the counting of AE events at a given location.

We recently proposed a probability-based analysis approach to estimate the amount of AE events locally, taking into account the stochastic nature of localization errors. In this approach, we define a parameter called the probability density of the location of AE events (pdAE), which represents the likelihood of the total amount AE events at a location. Locations with larger pdAE values have a higher chance of having more AE events. The pdAE at a random location $\mathbf{x}$ is calculated as

$$p_{\mathbf{A}}(\mathbf{x}) = \sum_{a\in\mathbf{A}} f\left(\mathbf{x}, \mathbf{x}_{\mathrm{g},a}\right) = \sum_{a\in\mathbf{A}} \frac{1}{\left(\sqrt{2\pi}\right)^k} \frac{1}{\sigma^k} e^{-\|\mathbf{x}-\mathbf{x}_{\mathrm{g},a}\|^2/2\sigma^2}, k \in \{1,2,3\} \tag{2}$$

where, $\mathbf{A}$ is a set of all AE events that occurred within the measurement time and spatial range, $\mathbf{x}_{\mathrm{g},a}$ is the estimated location of event a, k is the dimension of the measuring zone which could be 1D, 2D or 3D, σ is the standard deviation of the localization error component (which is assumed to be the same for all dimensions). We use $\sigma = 39$ mm based on a previous evaluation of source localization error in concrete structures. The details can be found in the authors' previous paper [29].

Fig. 2a exemplifies the pdAE field of one AE event a_1. Due to source localization error, this event can be estimated at any point in space with varying likelihood. The probability densities at two points p_1 and p_2 are 75.32 m^{-2} and 12.76 m^{-2} respectively. This indicates that the AE event has a higher chance of being located at p_1 than at p_2, which makes sense considering that p_1 is closer to the actual location than p_2. When more AE events occur, by superimposing the field of each event, we can obtain the pdAE field of all AE events. Fig. 2b exemplifies the pdAE field of

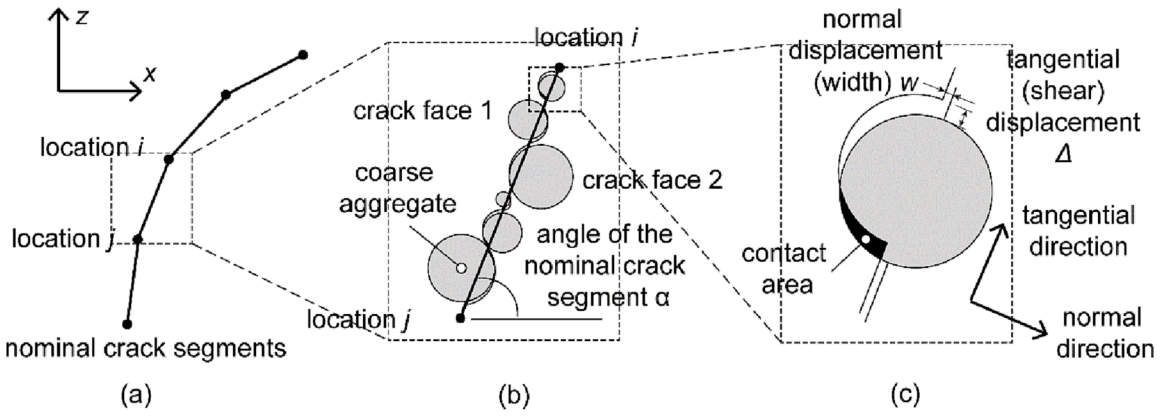

Fig. 1. Illustration of the crack kinematics at a location along a crack: (a) approximation of the crack pattern to nominal crack segments, (b) angle of a nominal crack segment and (c) crack kinematics at location *i*.

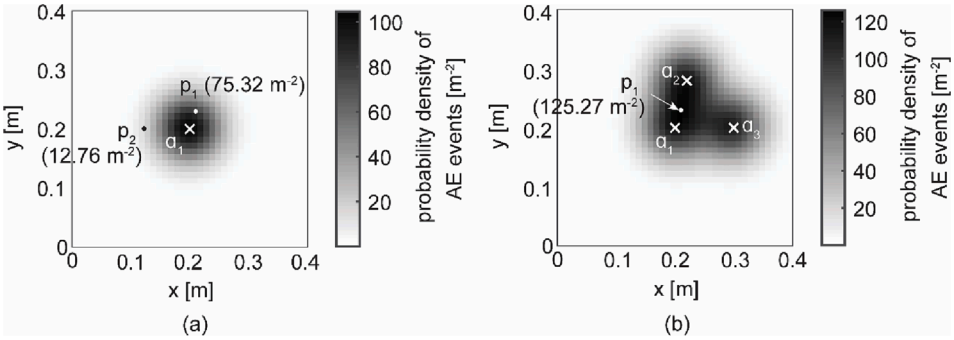

Fig. 2. Illustration of probability density field of (a) one AE event and (b) multiple AE events.

three AE events a_1, a_2 and a_3. The probability density at the same point p_1 increases to 125.27 m^{-2}, meaning that the likelihood of AE events being at point p_1 increases as more AE events occur. The integral over the entire space is equal to the number of AE events (which is 3 in our example).

Previous applications of this analysis method have demonstrated that the pdAE field can more effectively indicate crack patterns and rationally quantify the spatial distribution of AE events, taking localization error into account [32].

The AE data analysis method also incorporates a location-dependent source amplitude threshold. Fig. 3 presents an example of such a source amplitude distribution for a given sensor layout in test I123A (one of the tests used in this paper). The grey scale illustrates the minimum source amplitude required for an AE source to be localized. We observe lower values in the centre of the sensor grid compared to the edge (71 dB and 82 dB respectively). This means that at measuring locations near the centre, more AE events with lower source amplitude can be localized (those with source amplitudes below 82 dB and above 71 dB). The sensor layout is more sensitive to AE events originating near the centre of the layout. Detailed descriptions of calculating the required source amplitude for a given sensor layout can be found in Chapter 6 of the thesis of the author [33]. To ensure consistent sensitivity of AE events throughout the coverage volume of the AE sensors, we only consider AE events with a source amplitude above the maximum value in the required source amplitude distribution (which is 82 dB for the test I123A in Fig. 3).

3. Experiments

We apply the aforementioned methods to establish the pdAE-crack kinematics relationship in a series of failure tests of reinforced concrete beams. A total of five tests are used, named H601A, H602A, H603A, H604A and I123A. These tests were originally designed to study

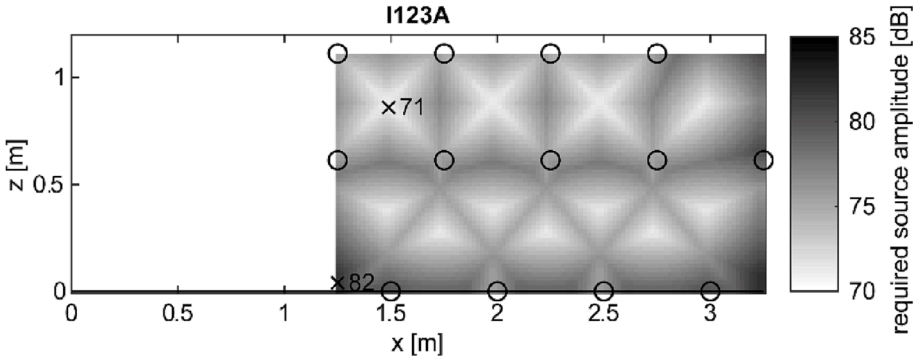

Fig. 3. Distribution of the required source amplitude for localization in test I123A.

the shear behaviour of reinforced concrete beams without shear reinforcement [34]. This section only introduces the test setups and the measurements related to the purpose of this paper.

3.1. Test setups

The five tests have similar setups. The dimensions of the beams are 10000 mm × 300 mm × 1200 mm. A commercial concrete mixture of C65 was used. Longitudinal reinforcements are present at the outer layers, where the tensile and compressive stress are at their maximum. Between the longitudinal reinforcement layers, only bulk unreinforced concrete is present. Fig. 4 shows the beam configuration and reinforcement layout. Except for test H602A, the beams were loaded in cycles. Fig. 6 shows the loading positions. The detailed material properties and loading history can be found in the experiment report [34].

3.2. Measurements

For DIC measurement, before loading, we applied a random speckle pattern on one side of the beam (Fig. 5b). The size of the speckles is about 1–2 mm. A high-resolution camera with 8688 × 5792 pixels was used to take photos during load testing. At every load step when the load was held, a minimum of three photos were taken. Additionally, two flashes were used to maintain sufficient and constant illumination. Detailed setups of the DIC measurement can be found in Zarate Garnica [30].

The AE sensors have a central frequency of 60 kHz [35]. The sensor was attached to the specimen surface using a steel holder, as illustrated in Fig. 5a. A grease-like material was used as a couplant between the sensor surface and the specimen surface [36]. The data acquisition system has 16 channels. The threshold level for recording an AE hit was set to 50 dB.

After installation, pencil lead break tests were conducted near the sensor to ensure sufficient coupling effect. A 2H grade pencil lead with a diameter of 0.3 mm was used. Coupling was considered adequate when the peak amplitude of the received signal exceeded 90 dB.

Before designing the AE sensor layout, preliminary measurements of wave speed and attenuation were taken. We estimated the wave speed to be around 4100 m/s and the material attenuation to be around 20 dB/m. The total wave attenuation is a combination of material attenuation and geometric spreading loss [37]. After 1 m, the total attenuation was 55 dB. Considering a source amplitude of 100 dB and a threshold level of 45 dB, the maximum sensor spacing was determined to be 1 m. Fig. 6 shows the AE sensor layout.

3.3. Combining the pdAE and the crack kinematics data

DIC measured the crack pattern on one side of the specimen in the *x*-*z* plane. Fig. 7a shows the crack pattern from DIC in test H601A at failure. We manually selected 10 measuring locations along every crack, from the crack tip to the bottom, to approximate the crack path (as exemplified in Fig. 7a). At each measuring location, we calculated the crack kinematics, including crack width and shear displacement, from the DIC measurements using the method outlined in Section 2.1.

Unlike DIC, which measured from the side surface, AE detected all signals originating from the entire cross-section of the beam. Since the width (*y*) dimension is small compared to length (*x*) and height (*z*), we localized the AE events in the 2D *x*-*z* plane. Fig. 7b illustrates the AE source locations in test H601A until failure (excluding those during unloading). Based on the estimated source locations, we calculated the pdAE field. Fig. 7c presents the pdAE field of all AE events. At a certain height, the local peak of pdAE aligns with the centre of the crack observed in the experiment. For example, at the height $z = 0.82$ m (marked in Fig. 7c), the pdAE distribution has five local peaks corresponding to the centres of the five cracks CR1-CR5 (shown in Fig. 7d).

It is important to note that the crack patterns measured by DIC and AE do not exactly match. Fig. 7c projects the measuring locations marked along the crack pattern by DIC (the black '×') onto the pdAE field. For example, at × = 2.75 m, $z = 0.82$ m (point *a*, highlighted as the red '×'), the local peak of pdAE is actually at × = 2.71 m. A deviation of 0.04 m is observed. This difference could result from variations in crack patterns in the width direction of the specimen, as DIC measured from the side surface while the pdAE indicates the average value of the entire volume in the width direction. We account for this variation by using the location of the nearest local peak of pdAE at the same height (*z*) as the correspondence to the measuring location from DIC.

Generally, no validated pdAE results were obtained in two regions of the specimens. One region is around the longitudinal reinforcement where distributed secondary cracks are present. The AE source localization error exceeds the tolerable limit due to multiple cracks in a sensor grid. Consequently, in this region, the crack pattern could not be clearly recognized by the pdAE field. The locations where pdAE could not clearly identify the crack patterns are circled in Fig. 7c. The other region

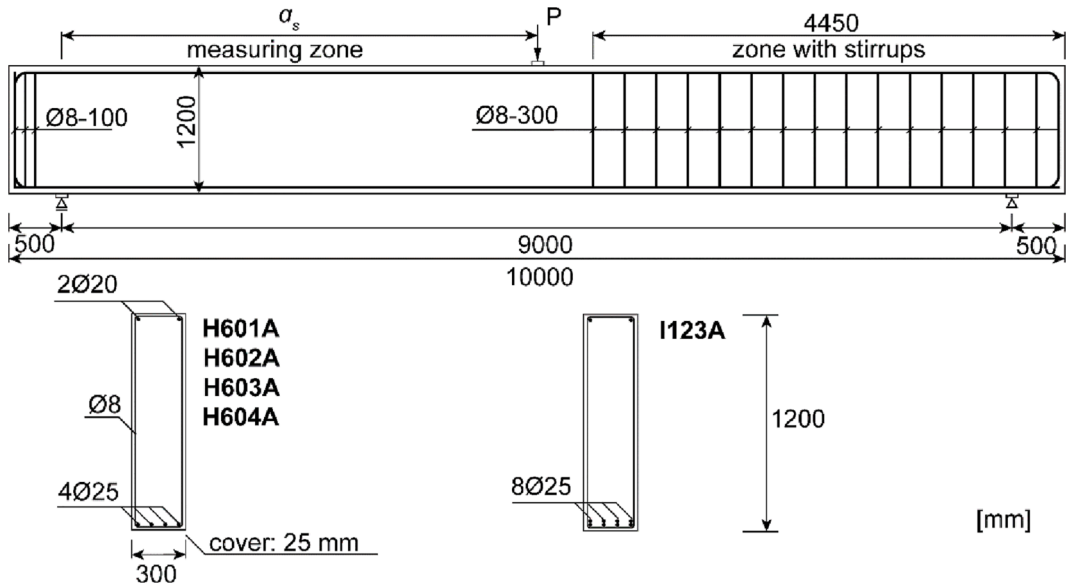

Fig. 4. A sketch of beam configuration including beam dimension, reinforcement layout and locations of supports and load.

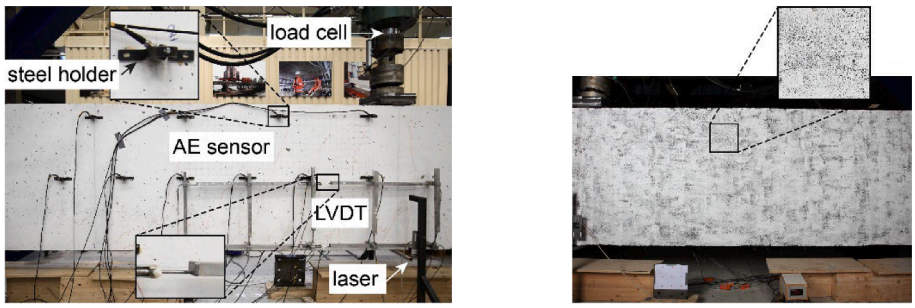

Fig. 5. Applied sensors in beam tests: (a) load cell, LVDTs, laser, AE sensors on one side and (b) DIC pattern on the other side (photos taken from test H601A).

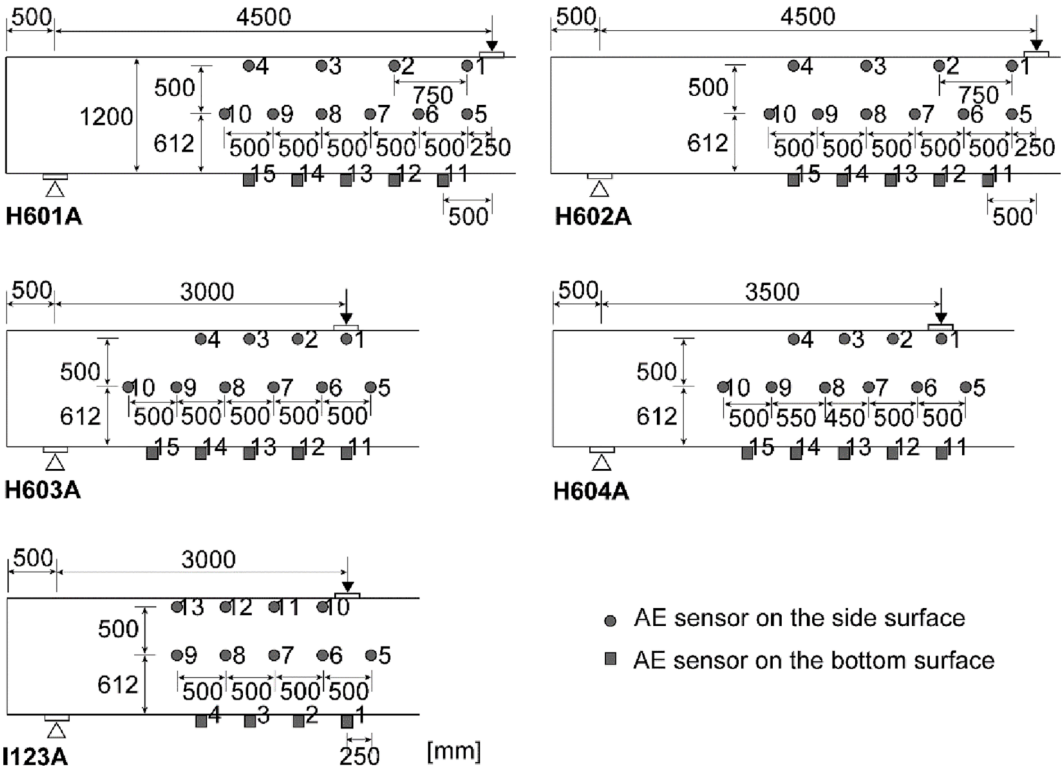

Fig. 6. AE sensor layout in the tests. The grey circle shows the AE sensor on the side surface and the grey rectangular shows the AE sensor on the bottom surface.

is near the edge of the AE measuring zone. When calculating the pdAE, an infinite space is assumed, which is not valid at the edge. Without clarifying the effect of assuming an infinite space at the edge, this paper excludes the points that are within 0.09 m to the edge (which takes the 95-percentile localization error from the simulation [29]).

After these adjustments, Fig. 7e displays the measuring locations where the pdAE and the crack kinematics from DIC are related in test H601A. They are numbered from the crack tip to the bottom. The black '×' indicates the measuring locations marked from DIC, and the white '+' shows the corresponding locations in the pdAE field. The same approach was applied to other tests.

Fig. 8 shows a schematic cyclic loading, where the paths of loading and unloading are marked in red and blue respectively. During loading, the pdAE considers the cumulative AE events from the start of test (which is marked in the figure). Correspondingly, the crack kinematics in the same part of loading path is considered. During each unloading path, the pdAE considers the cumulative AE events from the start of unloading in that path (marked in the figure). Accordingly, the crack kinematics is calculated.

4. Results

This section presents the obtained relationships between the pdAE and the crack kinematics at the measuring locations in the five tests. The relationships in the loading and unloading paths are reported separately (in Section 4.1 and Section 4.2).

4.1. Relationship between the pdAE and the crack kinematics during crack opening

Fig. 9 shows the relationship between the pdAE and the crack width during loading at the measuring locations of all the selected cracks of the specimens. A dotted line represents the change in the pdAE and the crack width at a measuring location with increasing load (Fig. 9b). For clarity, only the value at the maximum load level is marked (by the solid dot). Different lines indicate the relationships between the two parameters at various measuring locations.

The obtained pdAE-crack width relationships are categorized into three groups, coloured as red, yellow and green in Fig. 9a. With a same

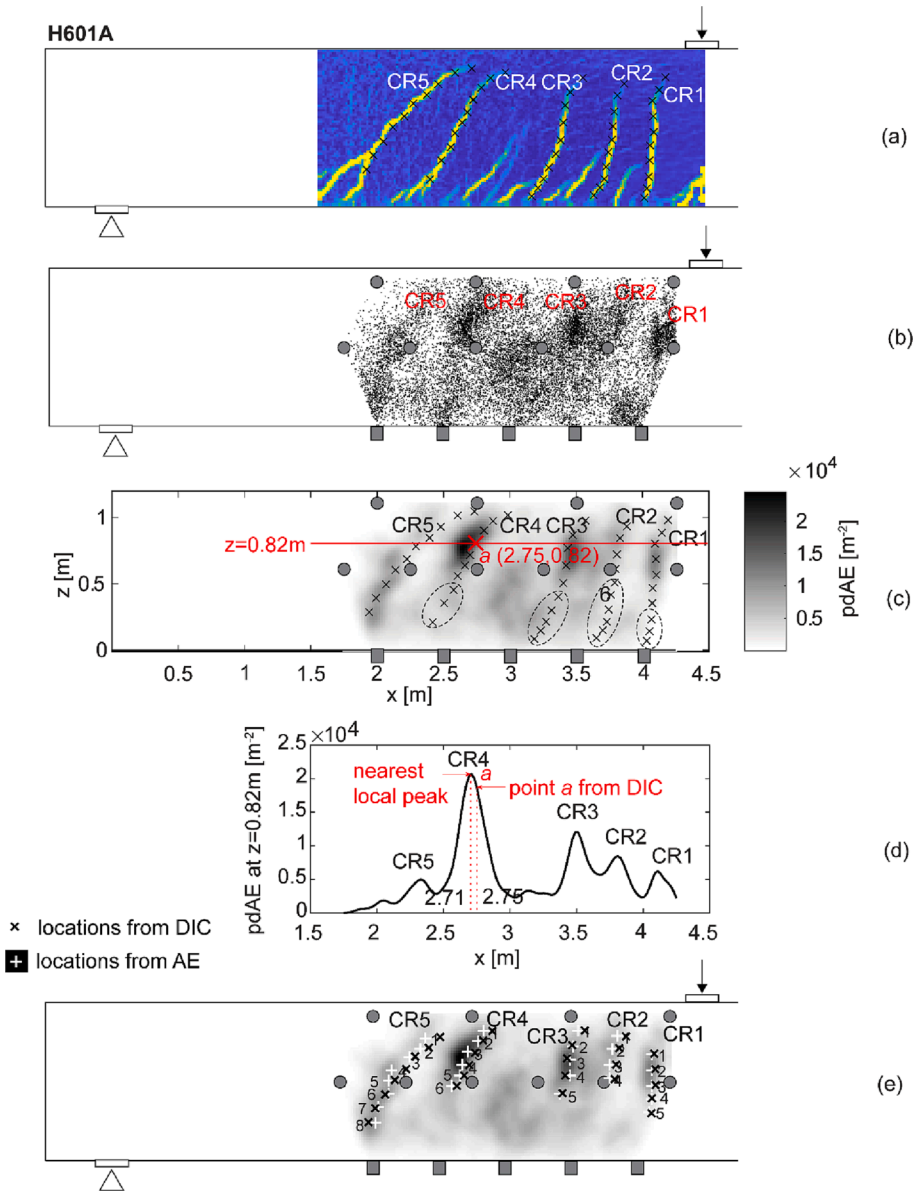

Fig. 7. Calibration of the crack patterns detected by DIC and AE in test H601A: (a) DIC crack pattern, where 10 measuring locations along each crack are selected, (b) estimated source locations until failure (excluding those during unloading), (c) pdAE field, with measuring locations from DIC projected, (d) pdAE distribution at $z = 0.82$ m, where the nearest local peak is used to find the corresponding location and (e) the measuring locations which are numbered from the crack tip. The 'x' marker shows the location from DIC, and the '+' marker shows the corresponding location from AE.

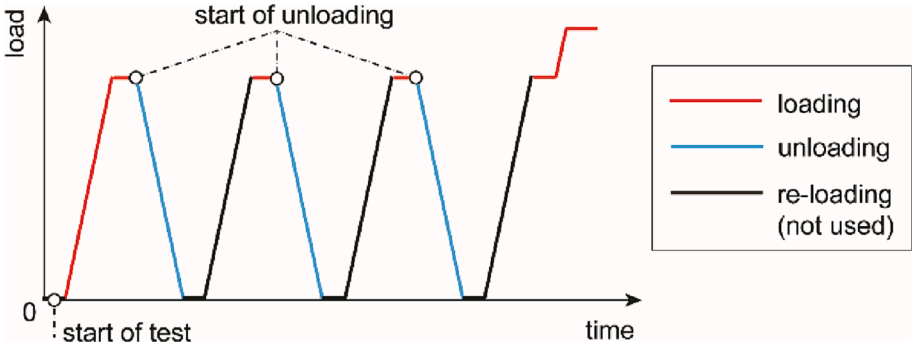

Fig. 8. A schematic cyclic loading history with one loading path and three unloading paths, to indicate the data organization during loading and unloading.

crack width, the pdAE is the largest in the red group and the smallest in the green group. The three groups are divided by two curves: $p_1 = 15000 \arctan(5w)$ and $p_2 = 7500 \arctan(5w)$, where w is the crack width and p is the pdAE. For every relationship (the dotted lines), the values of pdAE and crack width at the maximum load level (shown by the solid dot) determine the group to which the relationship belongs. Fig. 9b exemplifies the group determination at one measuring location. The pdAE and crack width at the maximum load are denoted as p_{max} and w_{max} respectively. The p_{max} divided by $\arctan(5w_{max})$ is 17,365, which is over 15,000; therefore, the relationship is categorized into the red

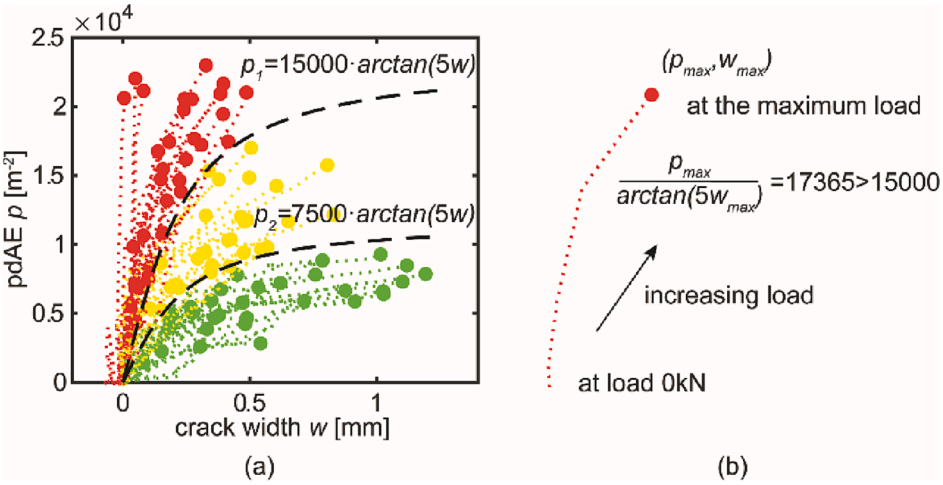

Fig. 9. Relationships between pdAE and crack width during loading: (a) at all the measuring locations and categorized into three groups: red, yellow and green, and (b) an example illustrating the group division. (For interpretation of the references to colour in this figure legend, the reader is referred to the web version of this article.)

group. The other relationships are categorized in the same manner.

Fig. 10 marks the measuring locations with the three groups of relationships. The colour of the markers corresponds to the group colour. We can find that the locations with green group relationships are mostly at cross-sections with larger bending moment over shear force ratios and at the bottom part of a cross-section (the tensile zone). The locations of markers belonging to the red group relationships are closer to the compressive zone of a cross-section. The locations of the yellow group are between the green and the red groups. This turns out to be a more general observation: the relationship between the pdAE and the crack width depends on the location of the measurement on the crack. Typically, with the same crack width, more AE events are expected at locations in the compressive zone than in the tensile zone, and more AE events are observed at cross-sections with larger shear force.

The dependency of the pdAE-crack width relationship on the location of measurement can be explained by the crack opening history. Fig. 11a displays the crack opening history (development of crack width and shear displacement during loading) obtained from DIC at the measuring locations of all the cracks in the tests. A dotted line shows the crack opening history at the same measuring location. For clarity, only the crack width and shear displacement at the maximum load level are marked (by the solid dot). According to the group that this measuring location belongs to, the colour of the line corresponds to the group colour. Generally, in the red group, a larger shear displacement occurs at a small crack width. While in the green group, the crack first opens wider, and slides gradually afterward. Some measuring locations in the red group are found to have negative crack width in the beginning. These locations are mostly in the compressive zone and were under compression before the crack tip reached the location.

When the crack first slides at a small crack width (the condition of the red group), the two crack faces are still in contact, resulting in more AE events from friction. When the crack first opens wide (the condition of the green group), the contact area between two crack faces is reduced. The subsequent sliding would generate less friction, thus fewer AE events.

Fig. 11b picks up three measuring locations, where similar crack width and shear displacement are observed at the maximum load level, but significantly different pdAE are obtained. The pdAE at the maximum load at these three measuring locations are given in the plot. Tracing back their crack opening history, we can find that at the location from the red group, more sliding first occurs at smaller crack width. Therefore, the amount of AE events is not only related to the absolute crack width, but also depends on the crack opening history.

To elaborate on this observation, we idealize the relationships between the pdAE and the crack width in Fig. 12 with two extreme hypothetical situations corresponding to the green and the red groups in Fig. 9-Fig. 11. Fig. 12a shows the relationships between the pdAE and the crack width. Fig. 12b shows the corresponding crack opening history. Fig. 12c shows the locations where these relationships may be found in a beam.

In Type I crack opening history, the crack faces initially move in the perpendicular direction of the crack path with limited sliding (corresponding to the green group). The pdAE increases with the crack width first and then stabilises. The stabilisation signifies a limited increase of pdAE. In this stage, the two crack faces make little contact, generating limited AE events. This type of cracking normally occurs in the tensile zone. The second extreme situation is defined as Type II crack opening history (corresponding to the red group). The crack faces slide simutaniously with opening, resulting in a significant increase in pdAE in the beginning. Afterwards, further opening would hardly increase pdAE. This type of crack opening history normally occurs in the compressive zone.

4.2. Relationship between the pdAE and the crack kinematics during crack closure

The relationship between pdAE and the crack kinematics during crack closure is studied using test I123A. In the initial cycle of reaching a load level, the unloading process was performed in steps (as shown in Fig. 13a). At each unloading step, DIC measurement was carried out to track the crack kinematics during unloading, which is used to compare to pdAE from the same part of the unloading path.

The authors note that in the ideal case the pdAE-crack kinematics during crack closure would be investigated for all five tests. However, except for test I123A, no stepwise unloading and related DIC measurements were performed for the other tests.

Fig. 13b and c show the two unloading paths and the incremental AE events at constant time steps in test I123A. These AE events are from the entire measuring zone, which describe the closure of existing cracks during unloading. At 250 kN, the existing cracks are CR2 and CR3, and at 300 kN, the existing cracks are CR2, CR3 and CR4. CR1 is not included as it is outside the measuring zone. The location of these cracks can be found in Fig. 10.

During unloading, we initially observe a limited increase in AE events. It is not until the load is reduced to a certain level that AE events begin to increase more noticeably. Further unloading leads to an even greater increase in AE events. This phenomenon may be linked to the increasing contact area between two crack faces during unloading, as

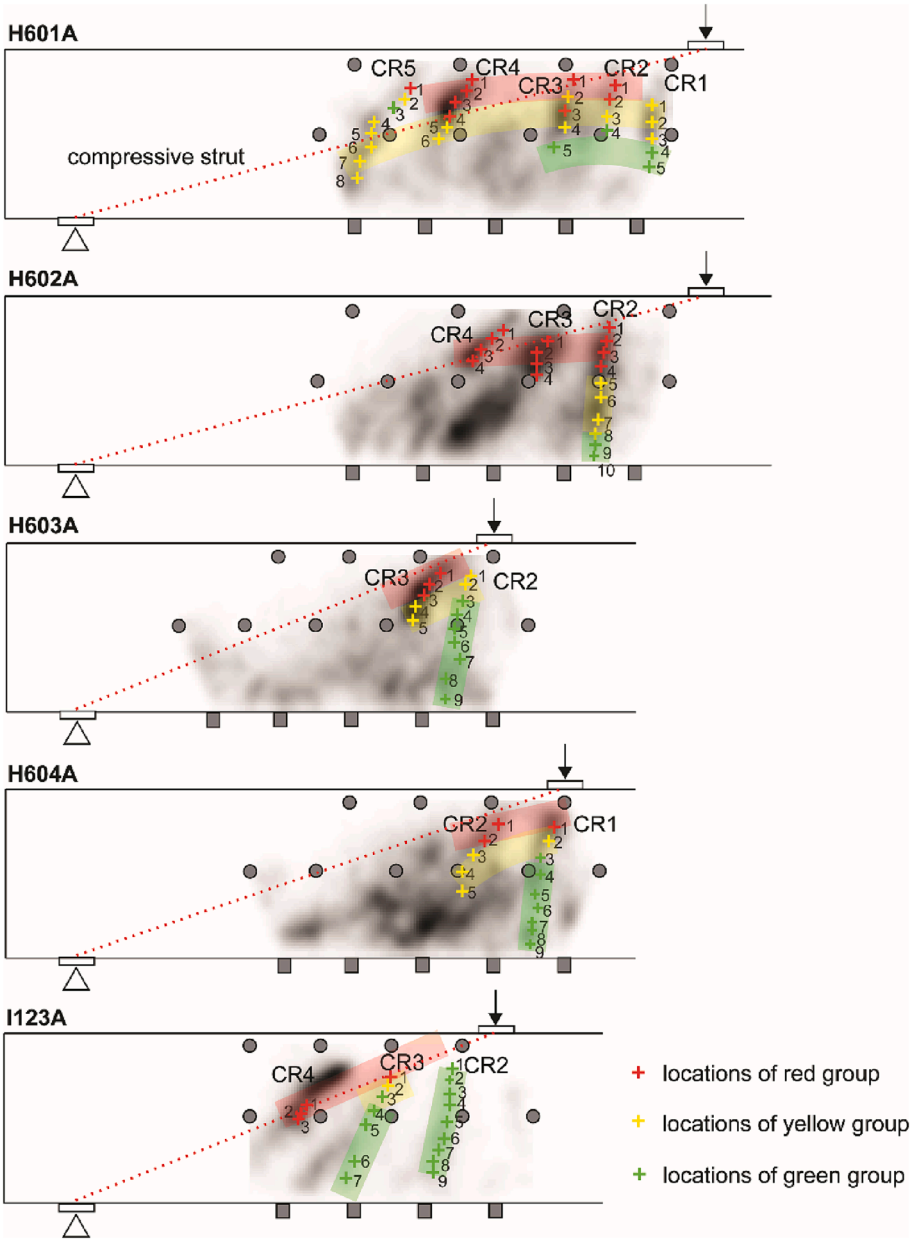

Fig. 10. The locations of the three groups. The dashed red lines indicate the estimated location of the compressive strut. The grey circles indicate the AE sensors on the side surface and the grey rectangles indicate the AE sensors on the bottom surface. (For interpretation of the references to colour in this figure legend, the reader is referred to the web version of this article.)

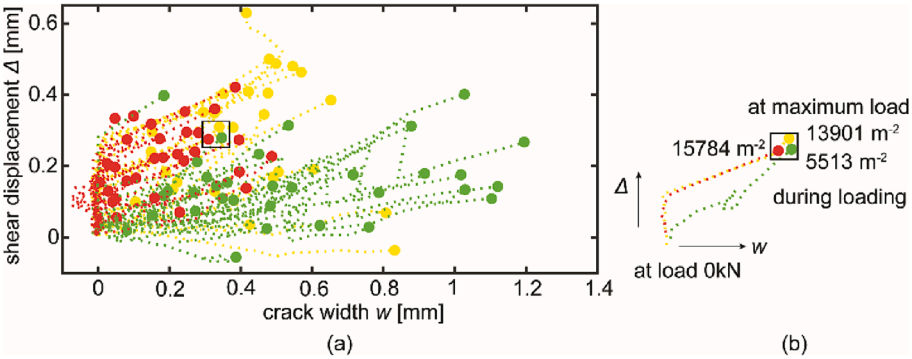

Fig. 11. Crack opening history during loading: (a) at all the locations of the three groups and (b) at one example from each group. The colour corresponds to the group colour.

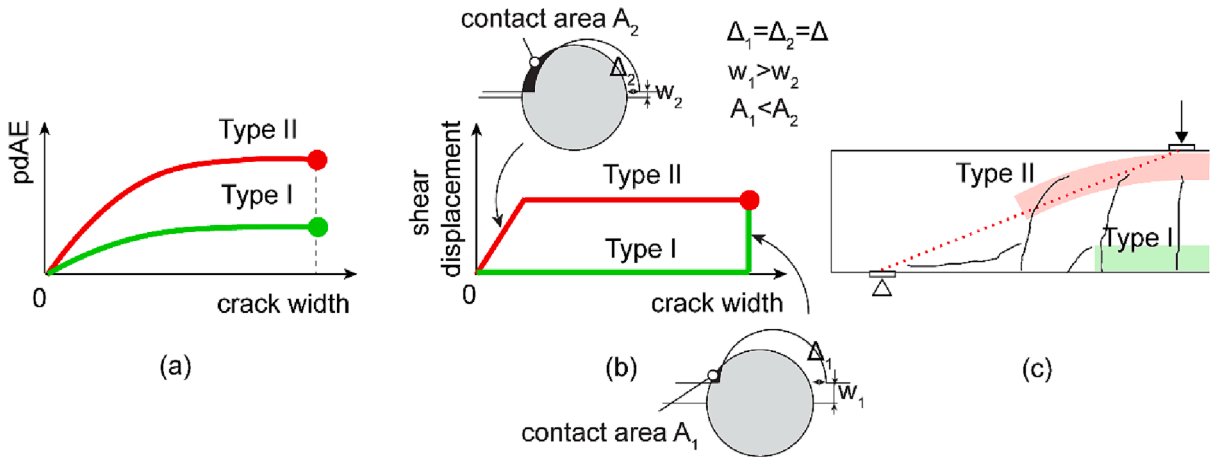

Fig. 12. Two extreme hypothetical situations Type I and Type II corresponding to the green and red groups respectively: (a) relationship between pdAE and crack width, (b) crack opening history and contact area at shear displacement Δ, (c) locations in a beam. (For interpretation of the references to colour in this figure legend, the reader is referred to the web version of this article.)

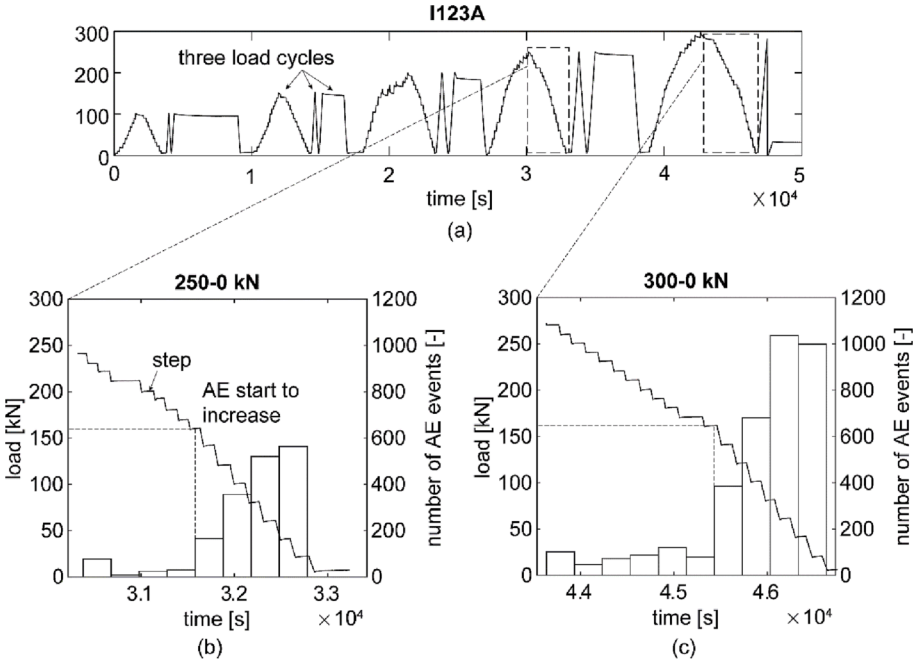

Fig. 13. (a) The studied unloading paths in test I123A, and incremental increase of AE events during unloading paths: (b) from 250 kN and (c) from 300 kN.

illustrated in Fig. 14. At the onset of unloading, the crack is at its maximum width, and the two crack faces barely make contact. As a result, minimal AE events are generated between the crack faces. This phase is referred to as the 'free closure stage' characterized by a lack of contact between crack faces. As unloading continues, the faces move closer until they make contact, causing AE events to increase. Further

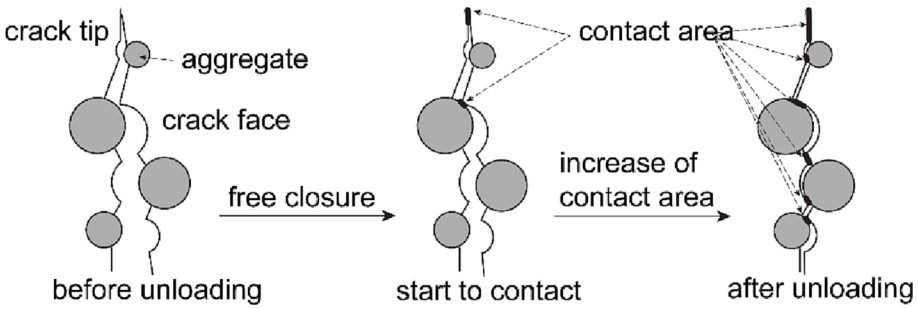

Fig. 14. Illustration of crack closure process: before unloading, the crack is widely opened without contact between two faces; the faces start to contact at a certain crack width; the contact area increases until fully unloaded.

closure reduces the crack width and enlarges the contact area between the crack faces. We hypothesize that a larger contact area results in a more significant increase in AE events.

After discussing the evolution of AE events during unloading in the entire measuring zone, we study the relationship between the pdAE and crack kinematics locally at the measuring points along a crack. Fig. 15 shows the relationship between the pdAE and crack width during unloading from 250 kN and 300 kN at the measuring locations along the two selected cracks CR2 and CR3. These cracks can be attributed to Type I crack in the opening stage, according to Fig. 10. Every line in Fig. 15 shows the relationship at one measuring location. We only mark the pdAE and crack width before unloading, at the onset of AE events and after unloading (by the dots):

- Before unloading, the crack width is at its maximum (denoted as w_m).
- During unloading, the crack width reduces, and we start to observe AE events when the crack width is reduced to w_0. The start of AE is determined by a pdAE threshold of 105 m^{-2}.
- After the specimen is completely unloaded, the crack width will not return to zero. The residual crack width is denoted as w_r.

When the maximum crack width w_m before unloading is large (for example, point 7 in Fig. 15a), the crack initially closes freely without the two faces making contact, generating few AE events. As a result, the crack width at the onset of AE events w_0 is smaller than w_m. When the maximum crack width w_m before unloading is small (for example, point 5 in Fig. 15a), the crack faces are already in contact at the beginning of unloading, leading to the immediate occurrence of AE events. The crack width at the onset of AE events w_0 is close to w_m.

The factor determining the onset of AE events during crack closure is the mismatch between the two crack faces. In the case of idealized smooth crack faces, there is no mismatch, so the two crack faces only make contact when fully closed. However, for most concrete cracks, the two crack faces cannot perfectly close due to mismatch. We call the crack width at which the two crack faces begin to make contact the mismatch width w_{mis}. When $w_m > w_{mis}$, the crack first closes freely, and AE events start to occur at the mismatch width w_{mis}. When $w_m \leq w_{mis}$, the two crack faces are already in contact at the beginning of crack closure, and AE events are generated immediately. Therefore, the crack width at which AE events start is limited by the minimum of the maximum crack width and the mismatch width ($w_0 \leq \min\{w_m, w_{mis}\}$).

Fig. 16 idealizes the relationship between the pdAE and crack width during crack closure of a flexural crack. When the maximum crack width is larger than the mismatch width (at location *i*), a free closure stage is present without contact between the two crack faces. AE events start after the crack width reduces to the mismatch width when the crack faces contact. When the maximum crack width is within the mismatch width (at location *j*), AE events start at the beginning of unloading.

5. Discussion

5.1. A potential physical model to relate AE events and concrete crack mechanisms

The pdAE-crack kinematics relationship observed during crack opening in Section 4.1 has clearly shown that the amount of AE events is not solely related to the crack opening in terms of crack width as most literature suggests. Instead, it relates to the complete crack kinematics during the opening history, including both crack opening and sliding. During crack sliding, friction at the localized contact areas between the two crack faces plays a significant role in generating AE events. As observed in Fig. 9a, the amount of AE events can increase by up to four

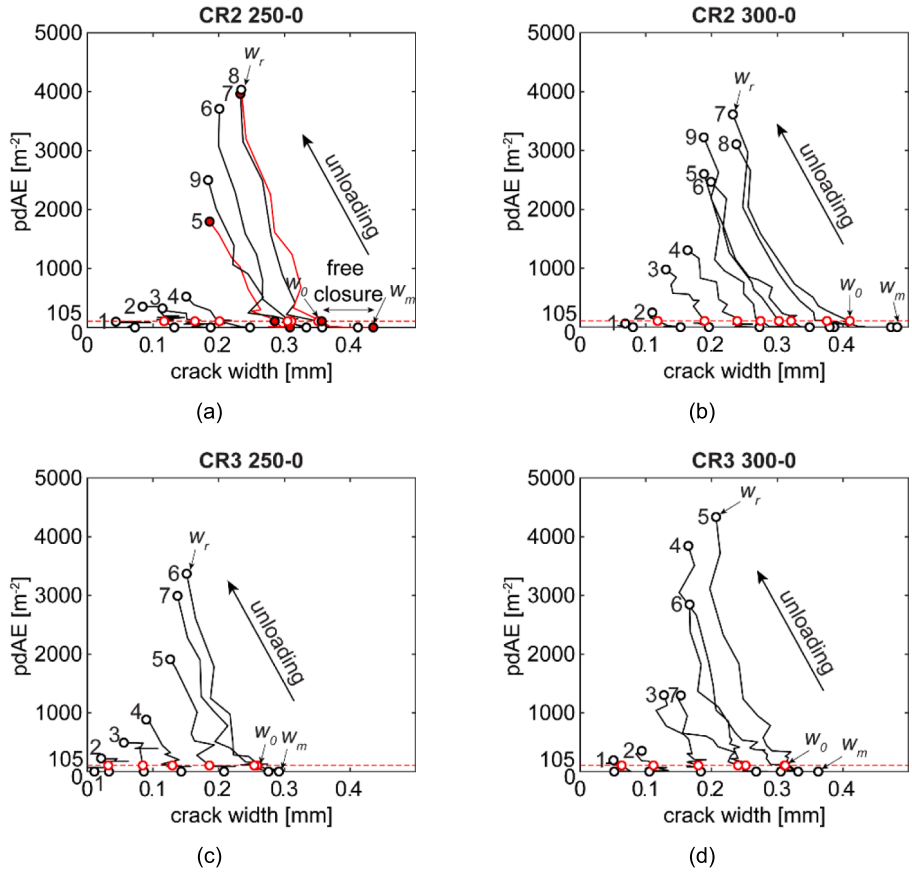

Fig. 15. Relationship between the pdAE and the crack width during crack closure in test I123A: (a) at points along CR2 at 250–0 kN, (b) at points along CR2 at 300–0 kN, (c) at points along CR3 at 250–0 kN and (d) at points along CR3 at 300–0 kN. The point number follows that in Fig. 10.

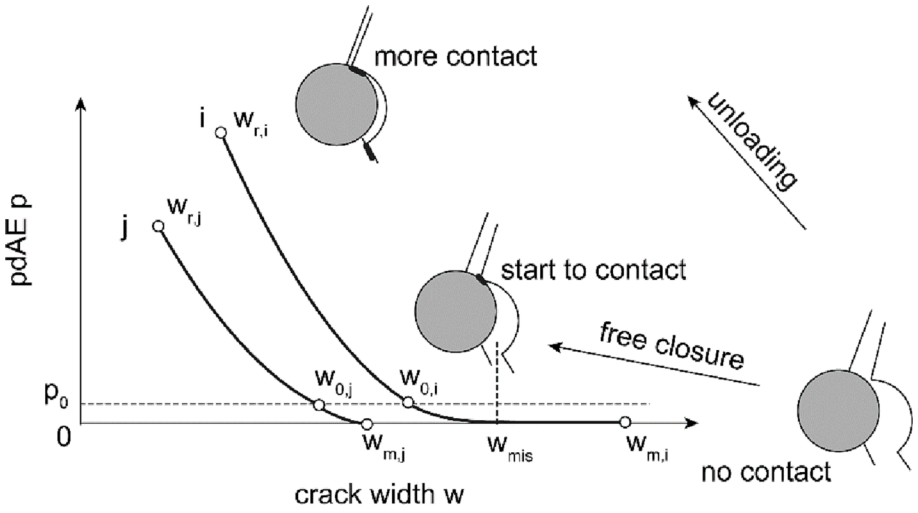

Fig. 16. Illustration of the relationship between the pdAE and the crack width during crack closure of a flexural crack.

times in some cases when comparing the results from the red group to those from the green group. This increase in AE events is attributed to the higher number of contact points between the crack faces, particularly when the crack width is small.

The influence of the contact area on the amount of AE events is also reflected in the observations made during crack closure in Section 4.2. AE events are only observed after the crack faces make contact, and the amount of AE events increases more with crack closure, likely due to a larger contact area. Previous research has also shown that the amount of AE events decreases with more load cycles [38], possibly due to the smoothening of crack surfaces and a reduction in mismatches, resulting in less contact during crack closure.

Therefore, we propose using the contact area to clarify the quantity of AE events generated by the friction (sliding) mechanism during crack opening and closure. We can differentiate AE events from friction based on distinct signal features using the method proposed by Zhang, Yang [39]. A potential physical model can be developed to associate the AE events from friction with the contact area. Various physical models have been presented in the literature to compute the contact area based on crack kinematics in the context of mechanical behaviour of cracks in concrete. One well-established model is the aggregate interlock theory [40]. In future work, we can connect the calculated contact area and the classified AE events from friction, which will essentially explain the quantity of AE events generated by friction.

5.2. A more rational use of AE to assess the concrete cracking

Assessment of concrete crack condition including the crack location and kinematics is important for the structural safety. The crack location can be determined by the localized AE events. Through the recently proposed parameter pdAE, the crack location can be identified with accuracy comparable to optical-based methods like DIC. The crack kinematics, on the other hand, is hard to be directly linked to the amount of AE locally. Nevertheless, insights from this paper help quantify the crack kinematics more rationally using AE.

The findings of this paper emphasize that crack width alone is not sufficient to explain the amount of AE events. Instead, a sound estimation of the amount of AE events should be based on the evolution of both the width and shear displacement. The contact area between the two crack faces is proposed as a potential parameter to indicate the amount of AE due to friction, which is also directly related to the mechanism of shear stress transfer along a crack according to the aggregate interlock theory [40].

Before developing a model that integrates the complete crack kinematics, most cases continue to primarily use crack width to evaluate the damage condition. Insights from this paper can also enhance the crack width estimation using AE for current cases. The pdAE-crack width relationship depends on the crack location within a structure, as demonstrated in Section 4.1. Relationship Type II should be considered when assessing cracking in the compressive zone of a concrete member, while Type I should be adopted for the tensile zone (as indicated in Fig. 13). If an equal amount of AE events are observed in both zones of a structure, the crack width in the compressive zone will be smaller than that in the tensile zone.

The tensile zone, typically located at the outer layer of a cross-section, allows for crack width measurement using sensors on the structural surface, such as LVDT and DIC. The measured surface crack width in the tensile zone can be used as a reference for estimating the internal crack width in the compressive zone, according to the pdAE-crack width relationships in both zones.

The pdAE-crack width relationship is rather consistent throughout the five specimens that were casted at different time and different batch of concrete. Nevertheless, it is necessary to recalibrate the approach for new tests involving concrete specimens with different reinforcement layouts, dimensions, or concrete mixtures. The methods presented in this paper can be used for recalibration, ensuring the applicability and adaptability of the approach in various scenarios.

6. Conclusion

This paper presents a detailed comparison between AE events and crack kinematics during crack opening and closure in large concrete beams. Thanks to the recently developed monitoring and data analysis techniques, namely DIC and pdAE, a detailed comparison between AE events and crack kinematics at each segment of a crack becomes possible for the first time in literature. This comparison provides a deeper understanding of the AE events generated during concrete crack opening and closure.

During crack opening, the relationship between pdAE and crack width depends on the evolutions of both width and shear displacement of the crack. Two types of crack kinematics and their respective relationships between pdAE and crack width are defined. Type I crack opening history, which often occurs in the tensile zone of a beam, generates fewer AE events due to less contact between crack faces during sliding. Type II crack opening history, often found in the compressive zone of a beam, generates more AE events due to more contact between crack faces at an early crack opening stage with an initially small crack width.

During crack closure, AE events do not occur until the crack width reduces to a certain value when the two crack faces contact. This value is

related to the mismatch of the two crack faces. Further reduction of crack width leads to more contact, generating more AE events.

Compared to the literature, we are able to explain the observed relationships between AE events and concrete crack kinematics with a clear physical background. The insights gained in this paper allow for a more rational use of AE to assess concrete cracking conditions. As a next step, we will study the relationship between crack kinematics and AE events by separating AE sources of tensile cracking and friction. AE events from tensile cracking are related to the creation of the crack faces. And AE events from friction are related to the friction at the contact. Potential physical models could be developed to relate AE events and the crack mechanisms more rationally.

Funding

This work was supported by Rijkswaterstaat, the Dutch Ministry of Infrastructure and Water Management.

CRediT authorship contribution statement

Fengqiao Zhang: Visualization, Writing – review & editing, Writing – original draft, Validation, Software, Methodology, Formal analysis, Data curation, Conceptualization. **Yuguang Yang:** Writing – review & editing, Supervision, Funding acquisition, Conceptualization. **Max A.N. Hendriks:** Resources, Writing – review & editing, Supervision, Project administration.

Declaration of Competing Interest

The authors declare that they have no known competing financial interests or personal relationships that could have appeared to influence the work reported in this paper.

Data availability

Data will be made available on request.

References

[1] E.O.L. Lantsoght, et al., Recommendations for the shear assessment of reinforced concrete slab bridges from experiments, Struct. Eng. Int. 23 (4) (2013) 418–426.
[2] Rijkswaterstaat, *Vervanging en Renovatie: Prognose voor de periode 2023 tot en met 2050*, in *forecast report*. 2022: the Netherlands.
[3] Muttoni, A. and M. Fernández Ruiz Shear strength of members without transverse reinforcement as function of critical shear crack width. 2008. **105, No 2**, 163-172-163-172.
[4] Y. Yang, J. Walraven, J.D. Uijl, Shear Behavior of Reinforced Concrete Beams without Transverse Reinforcement Based on Critical Shear Displacement, J. Struct. Eng. 143 (1) (2017) 04016146.
[5] Y. Yang, J. den Uijl, J. Walraven, Critical shear displacement theory: on the way to extending the scope of shear design and assessment for members without shear reinforcement, Struct. Concr. 17 (5) (2016) 790–798.
[6] N.V. Tue, W. Theiler, N.D. Tung, Schubverhalten von Biegebauteilen ohne Querkraftbewehrung, Beton- Stahlbetonbau 109 (10) (2014) 666–677.
[7] *fib*, *Monitoring and safety evaluation of existing concrete structures*. fib bulletin. Vol. 22. 2003: Elsener and Böhni.
[8] Grosse, C. and M. Ohtsu, *Acoustic emission testing: Basics for Research-Applications in Civil Engineering*. 2008.
[9] Grosse, C., et al., *Acoustic emission testing: Basics for Research-Applications in Engineering*. 2 ed. Springer Tracts in Civil Engineering. 2021, Switzerland: Springer Cham.
[10] T. Kundu, Acoustic source localization, Ultrasonics 54 (1) (2014) 25–38.
[11] M. Ohtsu, Recommendation of RILEM TC 212-ACD: Acoustic emission and related NDE techniques for crack detection and damage evaluation in concrete: Test method for classification of active cracks in concrete structures by acoustic emission, Mater. Struct. 43 (9) (2010) 1187–1189.
[12] M. Ohtsu, Recommendation of RILEM TC 212-ACD: Acoustic emission and related NDE techniques for crack detection and damage evaluation in concrete: Test method for damage qualification of reinforced concrete beams by acoustic emission, Mater. Struct. 43 (9) (2010) 1183–1186.
[13] L. Golaski, P. Gebski, K. Ono, Diagnostics of reinforced concrete bridges by acoustic emission, J. Acoustic Emission 2002 (20) (2002) 83–89.
[14] D.R. Huston, et al., Acoustic Emission Monitoring of Prestressed Girders during Fabrication and Transport, ACI Struct. J. 118 (2) (2021) 49–60.
[15] T. Shiotani, D.G. Aggelis, O. Makishima, Global Monitoring of Large Concrete Structures Using Acoustic Emission and Ultrasonic Techniques: Case Study, J. Bridg. Eng. 14 (3) (2009) 188–192.
[16] Yang, Y., D.A. Hordijk, and A. de Boer, *Acoustic emission measurement in the proof loading of an existing bridge affected by ASR*, in *5th International Symposium for Life-Cycle Civil Engineering*. 2016: Delft, the Netherlands.
[17] I. Bayane, E. Brühwiler, Structural condition assessment of reinforced-concrete bridges based on acoustic emission and strain measurements, J. Civ. Struct. Heal. Monit. 10 (5) (2020) 1037–1055.
[18] E.N. Landis, L. Baillon, Experiments to relate acoustic emission energy to fracture energy of concrete, J. Eng. Mech. 128 (6) (2002) 698–702.
[19] B.K.R. Prasad, R.V. Sagar, Relationship between AE Energy and Fracture Energy of Plain Concrete Beams: Experimental Study, J. Mater. Civ. Eng. 20 (3) (2008) 212–220.
[20] Srivastava, J., *Estimation of Energy Released from Crack in Concrete using Acoustic Emission and Comparison with the Numerical Results*. Master thesis, Delft University of Technology.
[21] N.B. Burud, J.M.C. Kishen, Response based damage assessment using acoustic emission energy for plain concrete, Constr. Build. Mater. 269 (2021), 121241.
[22] A. Carpinteri, et al., Cracking and crackling in concrete-like materials: A dynamic energy balance, Eng. Fract. Mech. 155 (2016) 130–144.
[23] A. Carpinteri, M. Corrado, G. Lacidogna, Heterogeneous materials in compression: Correlations between absorbed, released and acoustic emission energies, Eng. Fail. Anal. 33 (2013) 236–250.
[24] D.G. Aggelis, et al., Monitoring of the mechanical behavior of concrete with chemically treated steel fibers by acoustic emission, Constr. Build. Mater. 48 (2013) 1255–1260.
[25] G. Lacidogna, F. Accornero, A. Carpinteri, Influence of snap-back instabilities on Acoustic Emission damage monitoring, Eng. Fract. Mech. 210 (2019) 3–12.
[26] M. Ohtsu, Source kinematics of acoustic emission based on a moment tensor, NDT Int. 22 (1) (1989) 14–20.
[27] M. Ohtsu, T. Okamoto, S. Yuyama, Moment tensor analysis of acoustic emission for cracking mechanisms in concrete, Struct. J. 95 (2) (1998) 87–95.
[28] H.M. Westergaard, Bearing Pressures and Cracks, J. Appl. Mech. 6 (1939) A49–A53.
[29] F. Zhang, et al., Probability density field of acoustic emission events: Damage identification in concrete structures, Constr. Build. Mater. 327 (2022), 126984.
[30] Zarate Garnica, G., *Analysis of shear transfer mechanisms in concrete members without shear reinforcement based on kinematic measurements*. Master thesis, Delft University of Technology.
[31] F. Zhang, L. Pahlavan, Y. Yang, Evaluation of acoustic emission source localization accuracy in concrete structures, Struct. Health Monit. 19 (6) (2020) 2063–2074.
[32] F. Zhang, Y. Yang, M.A.N. Hendriks, Identification of internal damages in reinforced concrete slabs using probability density field of acoustic emission events, in: 35th European and 10th International Conference on Acoustic Emission Testing, Ljubljana, Slovenia, 2022, pp. 310–318.
[33] Zhang, F., *Acoustic emission-based indicators of shear failure of reinforced concrete structures without shear reinforcement*. PhD thesis, Delft University of Technology.
[34] Yang, Y., *Shear behaviour of deep RC slab strips (beams) with low reinforcement ratio*, in *Stevin Report*. 2020, Delft University of Technology: Delft, the Netherlands.
[35] MISTRAS, *R6I-AST Sensor*, in *Product Data Sheet*. 2008, MISTRAS Group Inc.: Princeton Junction, NJ 08550.
[36] MOLYKOTE, *MOLYKOTE 4 Electrical Insulating Compound*, in *Product Data Sheet*. 2018, DuPont de Nemours, Inc.
[37] Bormann, P., B. Engdahl, and R. Kind, *Seismic Wave Propagation and Earth models*, in *New Manual of Seismological Observatory Practice 2 (NMSOP2)*, P. Bormann, Editor. 2012, Germany: Deutsches GeoForschungsZentrum GFZ, 1-105.
[38] Zhang, F., Y. Yang, and M. Hendriks, *Acoustic Emission-based crack tracking for existing concrete structures: Influence of number of load cycles and loading speed*, in *10th International Conference on Bridge Maintenance, Safety and Management (IABMAS 2020)*. 2021, CRC Press, London: online.
[39] F. Zhang, et al., Developing a new acoustic emission source classification criterion for concrete structures based on signal parameters, Constr. Build. Mater. 318 (2022), 126163.
[40] J.C. Walraven, Fundamental analysis of aggregate interlock, ASCE J. Struct. Div. 107 (11) (1981) 2245–2270.